RESEARCH REPORTS
Biomaterials & Bioengineering

A. Rmaile[1]*, D. Carugo[2], L. Capretto[2], M. Aspiras[3], M. De Jager[4], M. Ward[3], and P. Stoodley[1,5]

[1]nCATS, Faculty of Engineering and the Environment (FEE), University of Southampton, UK; [2]Bioengineering Group, Faculty of Engineering and the Environment (FEE), University of Southampton, UK; [3]Philips Oral Healthcare Inc. (POH), Bothell, WA, USA; [4]Philips Oral Healthcare, Philips Research, Eindhoven, The Netherlands; and [5]Center for Microbial Interface Biology, Departments of Microbial Infection and Immunity, and Orthopaedics, The Ohio State University, Columbus, OH, USA; *corresponding author, ar1a09@soton.ac.uk

J Dent Res 93(1):68-73, 2014

Removal of Interproximal Dental Biofilms by High-velocity Water Microdrops

ABSTRACT

The influence of the impact of a high-velocity water microdrop on the detachment of *Streptococcus mutans* UA159 biofilms from the interproximal (IP) space of teeth in a training typodont was studied experimentally and computationally. Twelve-day-old *S. mutans* biofilms in the IP space were exposed to a prototype *AirFloss* delivering 115 µL water at a maximum exit velocity of 60 m/sec in a 30-msec burst. Using confocal microscopy and image analysis, we obtained quantitative measurements of the percentage removal of biofilms from different locations in the IP space. The 3D geometry of the typodont and the IP spaces was obtained by micro-computed tomography (μ-CT) imaging. We performed computational fluid dynamics (CFD) simulations to calculate the wall shear stress (τ_w) distribution caused by the drops on the tooth surface. A qualitative agreement and a quantitative relationship between experiments and simulations were achieved. The wall shear stress (τ_w) generated by the prototype *AirFloss* and its spatial distribution on the teeth surface played a key role in dictating the efficacy of biofilm removal in the IP space.

KEY WORDS: oral hygiene, *Streptococcus mutans*, micro-computed tomography, microscopy, interproximal cleaning, dental plaque.

DOI: 10.1177/0022034513510945

Received July 14, 2013; Last revision September 29, 2013; Accepted October 5, 2013

A supplemental appendix to this article is published electronically only at http://jdr.sagepub.com/supplemental.

INTRODUCTION

Good oral hygiene practice maintains a healthy oral cavity, controls the progress of dental plaque biofilms (ten Cate, 2006) and calculus, and prevents further complications such as gum diseases and tooth decay (Costerton *et al*., 1999; Jakubovics and Kolenbrander, 2010; Bjarnsholt *et al.*, 2011; Marsh *et al.*, 2011). The challenge of dental care products is to efficiently and quickly remove plaque from the interproximal (IP) space. Mechanical removal of IP plaque by traditional dental flossing products has been accompanied with bleeding, stuck or shredded floss, and prolonged flossing time (Darby, 2003). Fluid shear stress is an alternative mechanical approach for controlling biofilm build-up (Stewart, 2012). Previous studies have demonstrated that if sufficiently high fluid shear stress can be generated, this alone can stimulate biofilm detachment (Rutter and Vincent, 1988; Hope *et al*., 2003; Sharma *et al.*, 2005a; Paramonova *et al.*, 2009). High-velocity water droplets (Cense *et al*., 2006) and entrained air bubbles (Parini *et al*., 2005; Sharma *et al.*, 2005b) have also been shown to be able to remove bacteria and biofilms from surfaces utilizing the additional effect of generating a "surface-tension force" away from the surface by the passage of an air/water interface (Gómez-Suárez *et al*., 2001). An advantage of using fluid forces to remove biofilms is that mechanical forces can be projected beyond the device itself, by generating currents in the fluid surrounding the teeth by powered brushing (Adams *et al.*, 2002) or through the generation of water jets by oral irrigation (Lyle, 2011). However, continuous water jets have a disadvantage of requiring large reservoirs and can be messy to use because of the large volumes of water involved. More recently, the Sonicare™ *AirFloss* device has been introduced for removing IP plaque. The *AirFloss* shoots a microdrop volume of water and entrained air at a high velocity into the IP space in a discrete burst, thus creating high wall shear stress (τ_w) and high-impact pressure over short periods of time, minimizing water volume and cleaning times.

We previously reported the influence of high-velocity water microdrop impact on the detachment of artificial plaque from the IP spaces, to demonstrate how a real biofilm might detach (Rmaile *et al.*, 2013). Here, we go on to use the same *in vitro* model to look at bacterial biofilm removal and apply computational fluid dynamics (CFD) numerical techniques to model and predict the spatial distribution of fluid wall shear stress (τ_w) required to remove the biofilm. This paper reports the results of an experimental and numerical study on the influence of a high-velocity water microdrop impact on the detachment of *Streptococcus mutans* biofilms from the IP spaces of a typodont model.

MATERIALS & METHODS

Bacteria and Growth Media

Biofilms were grown from *S. mutans* UA159 (ATCC 700610). Stock cultures of *S. mutans* were stored at -80° C in 10% glycerol in physiological buffered saline (PBS). Biofilms were cultured with sucrose (2% w/v) supplemented brain heart infusion (BHI+S) medium (Sigma-Aldrich, Dorset, UK) and incubated at 37° C and 5% CO_2.

Typodont Model and Microburst

To recreate a realistic geometry associated with the IP space, we grew biofilms on the 2 upper central incisors (teeth 8 and 9) removed from a training typodont (A-PZ periodontal model 4030025, Frasaco GmbH, Tettnang, Germany) (Fig. 1A). A prototype *AirFloss* was used to generate a microburst of 115 µL (± 50; n = 30) over a time period of approximately 0.033 sec (Appendix I).

CLSM Microscopy and Image Analysis

The amount of biofilm on the IP surfaces of the typodont teeth was measured with a Leica TCS SP2 AOBS (Leica Microsystems, Nanterre, France) confocal laser scanning microscope (Fig. 2; Appendix II).

Micro-computed Tomography (μ-CT) Geometry Reconstruction of the Typodont Model

μ-CT was used to image the typodont in 3D and construct a model of the IP space to be used in subsequent CFD modeling (Fig. 1B; Appendix III).

Streptococcus mutans Biofilms inside Microfluidic Channels

To estimate a critical hydrodynamic shear stress required for *S. mutans* biofilm detachment, which could be used as a model input parameter for predicting the spatial distribution of biofilm removal, we used a BioFlux™ 1000 device (Fluxion Biosciences, South San Francisco, CA, USA) (Appendix IV).

Computational Fluid Dynamics Simulations

To model the dynamic behavior of the microburst created within the IP space, the tomography obtained from μ-CT was converted to a 3D computer-aided design (CAD) file geometry with Amira software (Mercury Computer Systems, Fürth, Germany). The computational domain, represented by the IP space, was discretized with software Gambit 2.4.6 (Symetrix Inc., Mountlake Terrace, WA, USA) and using a tetrahedral meshing scheme. A cell size of ~155 µm was chosen, which led to a total number of 143,985 mesh tetrahedral cells. Since the IP space was symmetrical, only half of it was modeled, reducing computational cost and time.

CFD simulations were performed with ANSYS Fluent 12.1.4 software (ANSYS Inc., Canonsburg, PA, USA), which allowed for the determination of the flow field within the IP space and τ_w generated on the tooth surface (Appendix V).

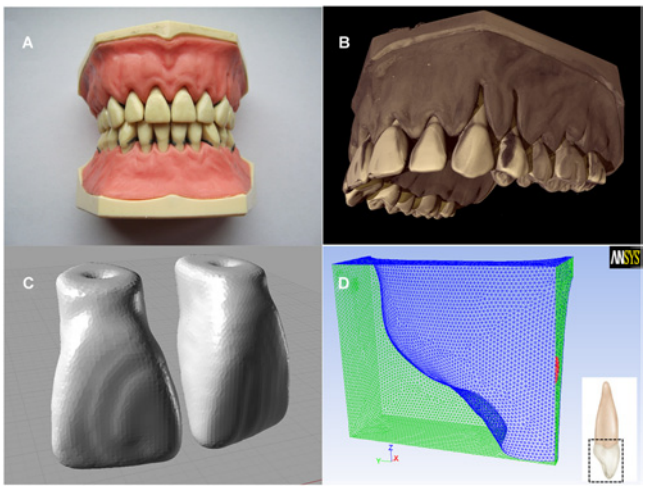

Figure 1. Digitization process of the training typodont. **(A)** Photograph showing the typodont used in the study. **(B)** Micro-CT image of the typodont (maxillary dental arch). **(C)** CAD-based 3D rendering of the IP space used in the study. **(D)** The 3D meshwork showing the geometry of the tooth surface that was used for the computational simulations. The sketch (right) shows the mesial view of a maxillary left central incisor, and the dashed square shows the region of interest used in the study.

Statistical Analysis

Statistical comparisons were made by one-way analysis of variance (ANOVA) (Excel 2003, Microsoft). Differences were reported as statistically significant for $p < .05$.

RESULTS

3D Imaging of Typodont Model

High-resolution 3D images detailing the micro-architecture of the typodont were obtained by *µ-CT* (Fig. 1B). This allowed us to computationally disassemble the typodont, maintaining the relevant juxtaposition between the individual teeth, and to create computational meshes of the teeth without interference from the other typodont materials.

Quantification of Biofilm Removal

With confocal microscopy, *S. mutans* biofilms grown in the IP space showed bacterial cells aggregating and forming complex cell cluster colonies consisting of 'tower'-, 'mushroom'-, and 'mound'-shaped structures. The thickness of the resulting biofilm on each tooth surface was approximately 200 to 300 µm. After the microburst, the images taken for the proximal surface of the teeth showed almost no biofilm close to the nozzle tip of the prototype *AirFloss*. Image analysis showed 95% removal close to the tip, 62% removal at approximately half the labio-palatal distance from the tip to the back of the teeth, and 8% removal at the back of the teeth (Fig. 3). The percentage removal values were plotted *vs.* the distance from the nozzle tip to the midpoint of the palatal surface of the teeth (Fig. 3A). The resulting curve was compared with the values obtained from the numerical simulations for τ_w at the same locations (Figs. 3C, 3D).

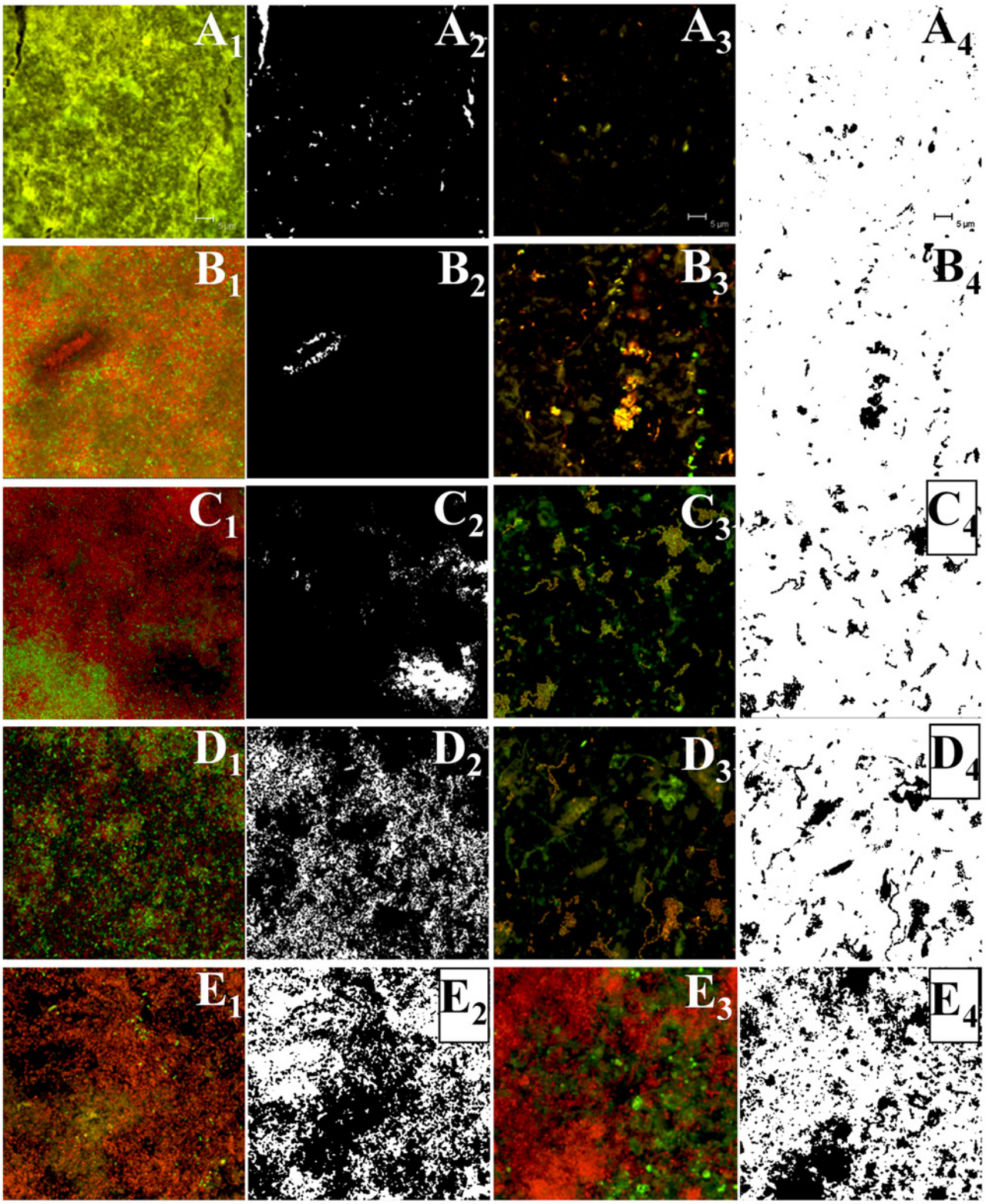

Figure 2. Representative CLSM images of *S. mutans* biofilm of 5 different locations **(A, B, C, D, E)** across the IP space at the level of the prototype *AirFloss* tip from the proximo-labial to the proximo-palatal side of a maxillary central incisor (the 5 locations are identified clearly in Fig. 3). **A_1, B_1, C_1, D_1,** and **E_1** are the images of the biofilm before the burst (on the untreated tooth), and **A_2, B_2, C_2, D_2,** and **E_2** are the corresponding images after thresholding with ImageJ (the biofilm is in black in these images, while the white areas are biofilm-free regions). Meanwhile, **A_3, B_3, C_3, D_3,** and **E_3** are the images of the biofilm on the treated tooth after the burst, and **A_4, B_4, C_4, D_4,** and **E_4** are the corresponding thresholded images. The untreated samples (columns 1 and 2) and treated samples (columns 3 and 4) are not from the same specimens. We calculated the % removal by subtracting the amount of biofilm that remained from the original amount of biofilm.

Critical Shear Stress for Biofilm-aggregate Detachment

The morphology of the biofilms in the BioFlux™ 1000 microfluidic channels varied markedly between one channel and the other, and also within the same channel. Structural heterogeneity is a common feature of biofilms. Nevertheless, common features could be noted, as seen by the microscopic images (Appendix Fig. 2): (i) the presence of individual bacteria and (ii) the presence of biofilm clusters of different sizes.

When τ_w was increased from 0 to 2 Pa, there was a slight increase in the overall detachment rate of the biofilm (Appendix Fig. 2), seemingly caused by adhesive failure (von Fraunhofer, 2012). The bacterial cells as well as the biofilm-aggregates appeared to slide along the surface before coming off. There was minimal detachment of the individual bacteria and the small aggregates over the applied elevated shear stress; but the larger biofilm clusters (with diameters over ~50 μm) detached when the shear stress ranged from 0.3 to 1.7 Pa. We extrapolated a conservative "critical biofilm-aggregates detachment shear stress" ($CDSS_{agg}$) of 1.7 Pa for the computational modeling. Above 2 Pa, the smaller biofilm clusters still appeared to be firmly attached to the substrate, and remained attached even after the shear stress was increased to 3 Pa.

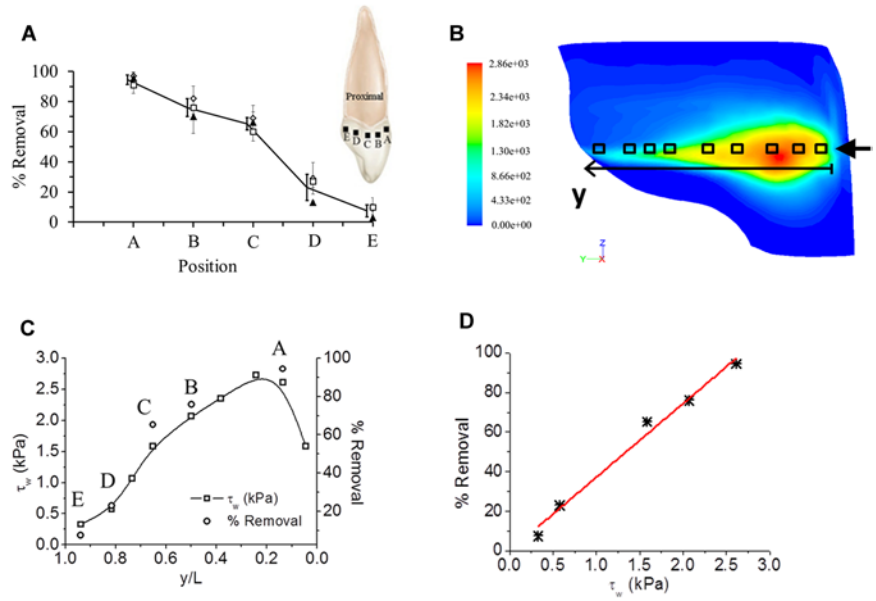

Figure 3. Biofilm removal as a function of shear stress and distance from the front of the tooth. **(A)** Percentage removal of the biofilm quantified from the CLSM images at 5 different locations on the tooth surface in the IP space. Three individual runs are shown by different symbols. The error bars represent standard deviations of the mean from 5 CLSM images. Solid line and heavy bars are the mean of the individual means (n = 3), which have been slightly offset for clarity. The schematic inset shows the proximal view of the upper central incisor, where the black squares represent the different locations where the CLSM images were taken. **(B)** Contour map showing the spatial distribution of τ_w on the tooth surface, as calculated from numerical simulations (circular nozzle tip; z/H = 0.5). The color bar is a linear scale showing the shear stress (Pa). **(C)** τ_w on the tooth surface (in kPa) at different y-positions along the tooth (*i.e.*, from labial to palatal side), at a fixed z-position (gingivo-incisal), as also calculated from numerical simulations. Empty squares correspond to the measurement points (squares) in 3B. On the secondary y-axis, the mean percentage removal measured experimentally in 3A (*i.e.*, solid line) is plotted, with the 5 empty circles (denoted as A, B, C, D, and E) corresponding to the same positions as in 3A. **(D)** Relationship between percentage removal (determined experimentally) and τ_w on the tooth surface (determined computationally). Datapoints were interpolated with a linear trend (red line).

Numerical Simulations

Mesh Independence Study

A mesh independence study was performed, and a cell size of 0.155 mm was selected for further numerical studies (Appendix V).

Quantification of Wall Shear Stress Distribution

A representative contour plot of the fluid τ_w spatial distribution on the tooth surface is shown in Fig. 3B. This simulation corresponded to a velocity inlet of 60 m/sec, with the circular nozzle tip located at z/H = 0.5, gingivo-incisally, where z (mm) is a spatial coordinate from the supragingival base of the tooth perpendicular to the tip of the tooth, and H (mm) is the supragingival height of the tooth. Thus, z/H = 0.5 equates to halfway up the tooth. The simulation showed the predicted fluid τ_w distribution on the proximal surface of the tooth, starting from the labial side of the IP space close to the nozzle tip (τ_w ~2.7 kPa), to the midpoint of the palatal surface of the tooth (τ_w ~0.3 kPa).

Computational Prediction of Shear Stress and Experimental Biofilm Removal

The τ_w distribution obtained computationally was compared with experimentally measured removal of biofilms. A linear correlation of % removal as a function of τ_w was found according to:

$$\text{Percent removal} = k\tau_w \ (r^2 = 0.94) \qquad (1)$$

where τ_w is wall shear stress (in Pa), and k (in Pa^{-1}) is the slope of the interpolating function (Figs. 3C, 3D).

Effect of the Nozzle z-position on Wall Shear Stress Distribution

Contours of fluid τ_w on the tooth surface at 5 nozzle tip z-positions were obtained to investigate the effect of tip positioning on the device's hydrodynamic performance. Fig. 4 shows the tooth surface area where τ_w is lower than the critical value of 1.7 Pa. Computational results predicted that the maximum % of

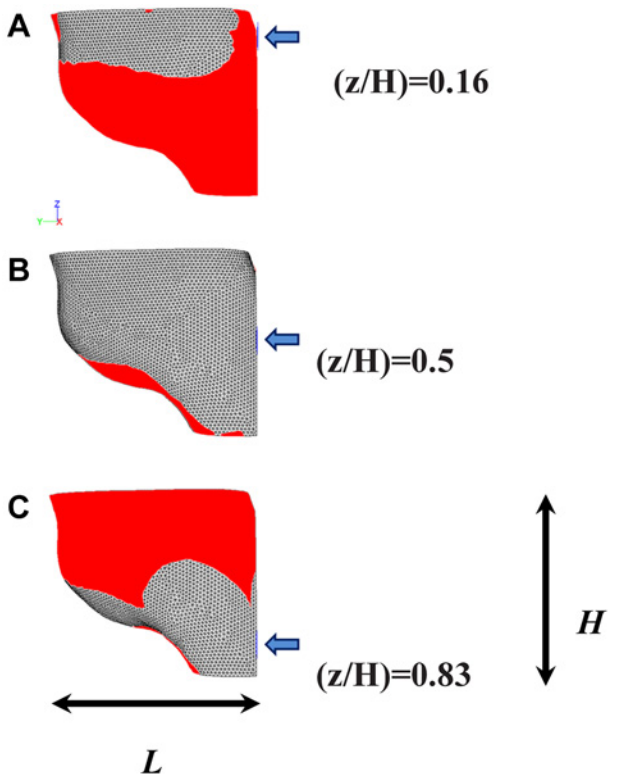

Figure 4. Effect of nozzle tip z-position (z/H) on fluid τ_w spatial distribution over the tooth surface. Tip cross-section is circular, and z/H was varied between 0.17 and 0.83 **(a-c).** The blue arrow indicates the flow direction. The red area corresponds to the tooth surface area where the shear stress is lower than $CDSS_{agg}$ = 1.7 Pa.

biofilm removal would take place when the nozzle tip is placed at z/H = 0.5 or z/H = 0.66, while the efficacy of biofilm removal would be significantly reduced at extreme z/H positions, namely, z/H = 0.17 (*i.e.*, close to the gum line) or z/H = 0.83 (*i.e.*, close to the incisal edge).

DISCUSSION

In the flow cell experiments, *S. mutans* biofilms were successfully grown inside microchannels under gravitational flow conditions. Under transmitted light microscopy (Appendix Fig. 2), the biofilm size and morphology showed resemblance to previously reported data (Costerton *et al.*, 1999; Heersink *et al.*, 2003). When the biofilm was subjected to an increased shear stress from 0 to 2 Pa, the large aggregates resisted movement from the surface until the wall shear stress reached a critical value, or $CDSS_{agg}$, which ranged between 0.3 and 1.7 Pa, at which they detached. However, even at this critical value, the smaller biofilm patches and individual bacterial cells remained attached. Generally, detachment of biofilm fragments (erosion), or even of the entire biofilm (sloughing), is caused by high flow shear stress levels that exceed the adhesion strength of the biofilm (Ohashi and Harada, 1994, 1996). The detachment of the large aggregates occurred at a relatively low shear stress (~1 Pa), while the smaller patches remained firmly attached, even after the flow increased up to 3 Pa. The *S. mutans* biofilms were grown under static or low shear conditions, thus leading to the formation of large cell aggregates, which tend to be approximately circular compared with the streamers that usually form under dynamic conditions. The streamlined shape has a significant effect on reducing the fluid drag on the elongated biofilms (Stoodley *et al.*, 1998, 1999). Streamers develop viscoelastic flexible bodies which oscillate rapidly when exposed to the flow forces, thus resisting detachment better than the large circular biofilm-aggregates grown at low laminar flow conditions. The large circular aggregates show different behavior under flow, with less ability to flex, resulting in detachment at lower fluid shear stress. This explains the experimentally observed detachment of the large aggregates at a relatively low shear stress (~1 Pa). So, the $CDSS_{agg}$ estimated here describes the detachment involving large aggregates only and not the total biofilm, which requires a higher critical shear stress for detachment, which was beyond the range of the microfluidics system under our operating conditions. The critical shear stress value of 1.7 Pa is close to the range of previously reported values of shear stress (5-12 Pa) required for detachment of non-dental biofilms (Ohashi and Harada, 1994; Stoodley *et al.*, 2002).

The exit velocity of the microdrops from the prototype *AirFloss* was 60 m/sec, and, based on earlier experiments, the flow was a steady stream (Rmaile *et al.*, 2013). Even though the shearing force was applied over very short periods of 30 msec, the generated fluid τ_w proved to be effective in removing the attached biofilm by both adhesive and cohesive failure (Rmaile *et al.*, 2013). However, fractions of the biofilm remained on the back of the teeth, due to tooth architecture and the fluid flow behavior in these regions, *i.e.*, the inability of the fluid to flow around the anatomical curvature and undercuts associated with the palatal surface of the upper central incisors. These observations were predicted by the computational simulations in which τ_w on the proximal surface of the teeth was observed to decrease gradually in the labio-palatal direction.

The simulations predicted τ_w distribution on the tooth surface caused by the microburst to be in the kPa range within the IP space, except in areas on the palatal side of the tooth, where τ_w became significantly lower (~200 Pa). The maximum computational values for the fluid τ_w were ~1,000 times higher than the $CDSS_{agg}$ obtained from the flow-cell experiments, and ~200 times higher than the estimated shear stress, reported in the literature, for biofilm detachment (Ohashi and Harada, 1994; Stoodley *et al.*, 2002). Thus, the simulations predict that a significant percentage area of the tooth is subjected to τ_w values capable of removing the plaque from the IP spaces. The large difference in adhesive strength between the 2 systems illustrates the importance of the physical growth conditions and surface type on adhesion strength. It was beyond the scope of this study to determine the influence of surface or hydrodynamics on adhesion strength. In mechanical testing, properties reports for the same species commonly vary by 3 orders of magnitude or greater (Shaw *et al.*, 2004). Whether this variability is true at different locations in the mouth or between patients is unknown, but measurements of the adhesion strength of real oral biofilm plaques would be useful in developing relevant *in vitro* models which look at mechanically induced detachment.

The 3D simulations for predicting τ_w were consistent with the experimental results obtained. As might be expected, the biofilm

survived the burst at areas of low τ_w, but was flushed away at areas where τ_w was higher. A linear relationship was found between the predicted fluid τ_w and the amount of detached biofilm obtained experimentally (Eq. 1). This relationship could be used to predict the efficacy of oral health care devices that use shear forces to remove plaque.

The computational model developed allowed for prediction of the effect of changing the position of the nozzle tip in the z-direction (inciso-gingivally) on biofilm removal efficacy. The numerical simulations predicted that placing the nozzle tip in or close to the middle of the inciso-gingival height (z/H = 0.5 or 0.67) provides more effective biofilm removal, in comparison with placing the tip closer to either the incisal edge or the gum line (Fig. 4). To the best of our knowledge, this is the first time that CFD has been used to calculate the wall shear stress distribution, caused by water drops generated from an oral hygiene device, on the tooth surface.

In this study, an experimental set-up was built and a methodology was developed to characterize, visualize, and quantify the efficacy of biofilm detachment by high-velocity water droplets, which prevents the accumulation of biofilm and automatically translates into prevention of dental caries formation at these sites.

ACKNOWLEDGMENTS

The use of both the IRIDIS High-Performance Computing Facility, and μ-VIS (CT centre), and associated support services at the University of Southampton is sincerely acknowledged. The authors also acknowledge Dr. Phil Preshaw from Newcastle University for helping with the development of the typodont model, Dr. Suraj Patel from labtech for helping with the BioFlux experiments, Dr. Philipp Thurner from the University of Southhampton for advice with μ-CT, and the late Dr. Hansjürgen Schuppe for helping with the CLSM images. This work was financially supported by Philips Oral Healthcare, Bothell, WA, USA. M. Aspiras and M. Ward are employed by Philips Oral Healthcare, Bothell, WA, USA. The other authors declare no potential conflicts of interest with respect to the authorship and/or publication of this article.

REFERENCES

Adams H, Winston MT, Heersink J, Buckingham-Meyer KA, Costerton JW, Stoodley P (2002). Development of a laboratory model to assess the removal of biofilm from interproximal spaces by powered tooth brushing. *Am J Dent* 15(Spec No):12B-17B.

Bjarnsholt T, Jensen P, Moser C, Høiby N (2011). Human oral bacterial biofilms: composition, dynamics, and pathogenesis. *In: Biofilm infections*. New York, NY: Springer, pp. 35-68.

Cense AW, van Dongen ME, Gottenbos B, Nuijs AM, Shulepov SY (2006). Removal of biofilms by impinging water droplets. *J Appl Phys* 100:124701.

Costerton JW, Stewart PS, Greenberg EP (1999). Bacterial biofilms: a common cause of persistent infections. *Science* 284:1318-1322.

Darby M (2003). Dental hygiene theory and practice. 2nd ed. Philadelphia, PA: WB Saunders.

Gómez-Suárez C, Busscher HJ, van der Mei HC (2001). Analysis of bacterial detachment from substratum surfaces by the passage of air-liquid interfaces. *Appl Environ Microbiol* 67:2531-2537.

Heersink J, Costerton WJ, Stoodley P (2003). Influence of the Sonicare toothbrush on the structure and thickness of laboratory grown *Streptococcus mutans* biofilms assessed by digital time-lapse and confocal microscopy. *Am J Dent* 16:79-83.

Hope CK, Petrie A, Wilson M (2003). In vitro assessment of the plaque-removing ability of hydrodynamic shear forces produced beyond the bristles by 2 electric toothbrushes. *J Periodontol* 74:1017-1022.

Jakubovics NS, Kolenbrander PE (2010). The road to ruin: the formation of disease-associated oral biofilms. *Oral Dis* 16:729-739.

Lyle DM (2011). Use of a water flosser for interdental cleaning. *Compend Contin Educ Dent* 32:78, 80-82.

Marsh PD, Moter A, Devine DA (2011). Dental plaque biofilms: communities, conflict and control. *Periodontol* 2000 55:16-35.

Ohashi A, Harada H (1994). Adhesion strength of biofilm developed in an attached-growth reactor. *Water Sci Tech* 29:281-288.

Ohashi A, Harada H (1996). A novel concept for evaluation of biofilm adhesion strength by applying tensile force and shear force. *Water Sci Tech* 34:201-211.

Paramonova E, Kalmykowa OJ, van der Mei HC, Busscher HJ, Sharma PK (2009). Impact of hydrodynamics on oral biofilm strength. *J Dent Res* 88:922-926.

Parini MR, Eggett DL, Pitt WG (2005). Removal of *Streptococcus mutans* biofilm by bubbles. *J Clin Periodontol* 32:1151-1156.

Rmaile A, Carugo D, Capretto L, Zhang X, Wharton JA, Thurner PJ, *et al*. (2013). Microbial tribology and disruption of dental plaque bacterial biofilms. *WEAR* 306:276-284.

Rutter PR, Vincent B (1988). Attachment mechanisms in the surface growth of microorganisms. In: Physiological models in microbiology. Vol. II. Bazin MJ, Prosser JI, editors. Boca Raton, FL: CRC Press, pp. 87-107.

Sharma PK, Gibcus MJ, van der Mei HC, Busscher HJ (2005a). Influence of fluid shear and microbubbles on bacterial detachment from a surface. *Appl Environ Microbiol* 71:3668-3673.

Sharma PK, Gibcus MJ, van der Mei HC, Busscher HJ (2005b). Microbubble-induced detachment of coadhering oral bacteria from salivary pellicles. *Eur J Oral Sci* 113:326-332.

Shaw T, Winston M, Rupp CJ, Klapper I, Stoodley P (2004). Commonality of elastic relaxation times in biofilms. *Phys Rev Lett* 93:098102.

Stewart PS (2012). Mini-review: convection around biofilms. *Biofouling* 28:187-198.

Stoodley P, Lewandowski Z, Boyle JD, Lappin-Scott HM (1998). Oscillation characteristics of biofilm streamers in turbulent flowing water as related to drag and pressure drop. *Biotechnol Bioeng* 57:536-544.

Stoodley P, Lewandowski Z, Boyle JD, Lappin-Scott HM (1999). Structural deformation of bacterial biofilms caused by short-term fluctuations in fluid shear: an in situ investigation of biofilm rheology. *Biotechnol Bioeng* 65:83-92.

Stoodley P, Cargo R, Rupp CJ, Wilson S, Klapper I (2002). Biofilm material properties as related to shear-induced deformation and detachment phenomena. *J Ind Microbiol Biotechnol* 29:361-367.

ten Cate JM (2006). Biofilms, a new approach to the microbiology of dental plaque. *Odontology* 94:1-9.

von Fraunhofer JA (2012). Adhesion and cohesion. *Int J Dent* 2012:951324.